

Communication

Liquid Crystal Tunable Dielectric Metamaterial Absorber in the Terahertz Range

Shenghang Zhou ¹, Zhixiong Shen ^{1,2}, Ruiyun Kang ³, Shijun Ge ^{1,2,*} and Wei Hu ^{1,2,*} 

¹ Key Laboratory of Intelligent Optical Sensing and Manipulation, College of Engineering and Applied Sciences, Nanjing University, Nanjing 210093, China; njuzsh@163.com (S.Z.); njuzxshen@163.com (Z.S.)

² Institute for Smart Liquid Crystals, JITRI, Changshu 215500, China

³ Beijing New Oriental Foreign Language School at Yangzhou, Yangzhou 225006, China; ruiyunkang@126.com

* Correspondence: geshijun@nju.edu.cn (S.G.); huwei@nju.edu.cn (W.H.)

Received: 30 October 2018; Accepted: 8 November 2018; Published: 10 November 2018



Abstract: In this paper, we propose a tunable dielectric metamaterial absorber in the terahertz (THz) range. The absorber is composed of a silicon pillar array embedded in a liquid crystal (LC) layer, which is sandwiched by two graphene electrodes. By way of varying the applied bias, the LC orientation can be continuously tuned. At a saturated bias, all LCs are vertically driven, and an absorption peak of 0.86 is achieved at 0.79 THz. When the bias is turned off, the same LCs are horizontally aligned, and the absorption peak degenerates into two smaller ones. A 47% modulation depth at 0.79 THz is obtained via numerical simulation with experimental feasibility considered. Such an active THz dielectric absorber may be utilized as part of various active THz apparatuses in THz imaging, sensing, switching, and filtering.

Keywords: dielectric absorber; liquid crystal; metamaterial; tunable; terahertz

1. Introduction

Terahertz (THz) waves, the last exploited part in the electromagnetic spectrum, have great potential in security screening [1], biological detection [2], and wireless communication [3]. Among various THz devices, an absorber that can efficiently capture wave energy is of vital importance. Metamaterial absorbers (MMAs) have drawn particular attention due to its capability of arbitrary frequency and amplitude modulation via freely designing their geometry [4]. After Tao et al. presented the first THz metallic MMA in 2008 [5], a tremendous amount of research on MMAs have been performed [6]. Integrated with functional materials including phase-change media [7], semiconductors [8], graphene [9], and liquid crystals (LCs) [10,11], MMAs exhibit tunable electromagnetic responses. The metals used in traditional metallic MMAs are often the highest electrically conductive materials in order to achieve high-Q resonance in MMAs. High electrical conductivity leads to high thermal conductivity and subsequently high ohmic loss. For applications where thermal properties are vital—e.g., THz imaging, sensing, and filtering—metal-free devices are preferred. To address this issue, Liu et al. developed a dielectric THz absorber based on hybrid dielectric waveguide resonances [12] and achieved an absorption of 97.5%. The functionality of this absorber is static. To further exploit dielectric MMAs with dynamic functions is meaningful.

LC presents excellent electro-optic tunability thanks to its broadband large birefringence and external field responsibility. Through spatially controlling the tilt or azimuthal directors of LC, the dynamic phase or geometric phase of THz wave can be freely manipulated [13,14]. However, these components all require a large LC thickness to accumulate sufficient phase retardation, leading to a slow response and high operating voltage. Recently, on the basis of the distinct influence on the resonance of metamaterials of surrounding LC refractive index change, various active THz

metadevices have been demonstrated, such as active filters [15,16], polarization converters [17], and phase shifters [18]. Here, both the cell gap and the operating voltage are drastically decreased. Through precisely designing the geometry of metadevices and optimizing the matching between the refractive index change of LC and electromagnetic resonant boundary condition, a dynamic tuning with large modulation depth can be reached.

Here, we propose a tunable THz dielectric MMA, which is composed of a silicon pillar array embedded in an LC layer driven by graphene electrodes. The function of this absorber relies on the overlapping between electric and magnetic dipole resonances of the silicon pillar array. We precisely set the radius of the pillar to satisfy the boundary condition at the bias saturated state, thus it behaves as a perfect absorber. While turning off the bias, the overlapped resonances are broken due to the refractive index change of LC. As a result, the absorption peak is split and its amplitude drops to half of the original one.

2. Tunable Dielectric Metamaterial Absorber

The configuration of the absorber is illustrated in Figure 1a. Both substrates were 500- μm -thick fused silica and covered with graphene electrodes. One of them could be spincoated with a 5- μm -thick polydimethylsiloxane (PDMS) film. The silicon pillar array could be fabricated on a 60- μm -thick heavily-doped silicon on insulator (SOI) using a Bosch process. Then it was bonded to the substrate with oxygen-plasma-treated PDMS [19]. Subsequently, the top SOI handle was stripped off with a lateral force. The unit geometry of the silicon pillar array is shown in Figure 1b. The PDMS layer separated the pillar array from the graphene electrode and worked as a refractive index matching layer simultaneously. Both substrates could be spincoated with a sulfonic azo dye (SD1) alignment layer, and then separated by a 110- μm -thick Mylar film to form the cell [20], as shown in Figure 1a. Finally, a home-made high-birefringence LC NJU-LDn-4 with $n_0 = 1.59 + 0.006i$ and $n_e = 1.90 + 0.001i$ around 0.80 THz could be infiltrated [21] to obtain the tunable THz dielectric MMA.

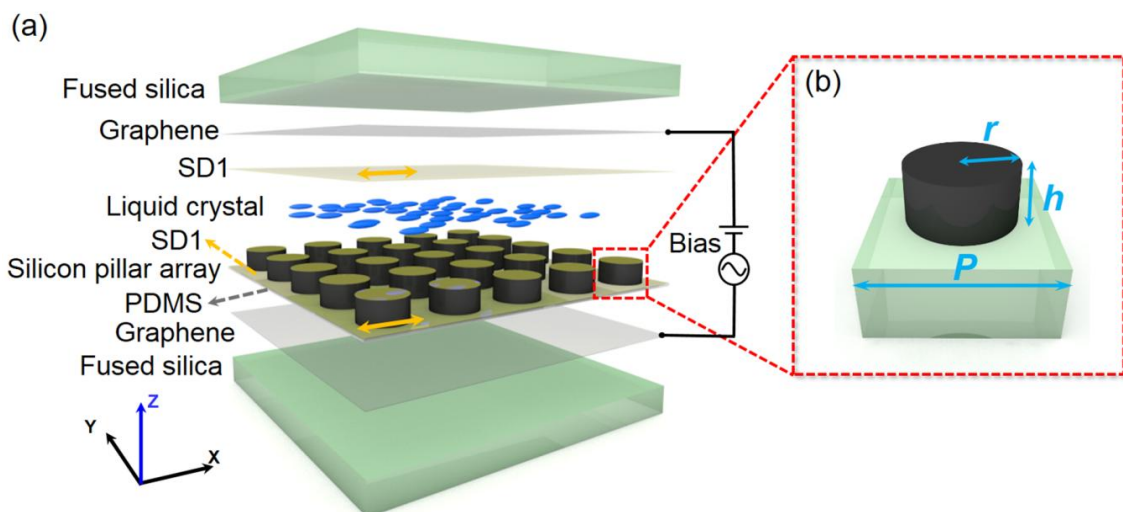


Figure 1. (a) The decomposition diagram of the LC integrated dielectric MMA. The yellow arrows indicate the alignment direction. (b) The unit dimension of the pillar resonator: lattice periodicity, P : 210 μm ; radius, r : 64 μm ; height, h : 60 μm .

We use hybrid dielectric waveguide resonances to explain the principle of this absorber. When the THz wave is incident along the z -axis (Figure 1a), the dielectric pillar works like a common waveguide. The resonator supports two different groups of hybrid modes, HE and EH. For HE mode, $H_z/E_z \ll 1$; while for EH mode, $E_z/H_z \ll 1$. Three dimensions of the field variation in the silicon pillar are denoted by different indices, i.e., HE_{nml} and EH_{hml} . Here, only the lowest magnetic dipole mode (HE_{111}) and electric dipole mode (EH_{111}) are taken into account [22]. Each pillar is represented by an ideal Huygens'

source, i.e., a pair of electric and magnetic dipoles oriented in the x - (EH_{111}) and y - (HE_{111}) direction respectively [23]. When both resonances occur at the same frequency, impedance matching is satisfied, which means the THz wave is totally absorbed. HE_{111} always exists for a given resonator, while EH_{111} has a cutoff condition. At a resonance wavelength of λ_0 , the cut off condition for a pillar dielectric resonator is given by [24]:

$$r = 0.61 \frac{\lambda_0}{(n_{Si}^2 - n_{LC}^2)^{1/2}} \quad (1)$$

Wherein, r is the radius of the pillar, and n_{Si} and n_{LC} are the refractive indices of silicon and surrounded LC respectively. For the lowest modes, the desired minimum height h of the resonator can be approximated as a half-wave dipole with

$$h = \frac{\lambda_0}{2n_{Si}} \quad (2)$$

Therefore, the pillar parameters are set as shown in Figure 1 to ensure both HE_{111} and EH_{111} are supported at the same frequency when the surrounding refractive index was 1.59 (bias saturation state). After turning off the bias, the surrounding refractive index increased to 1.90, inducing the cutoff of EH_{111} . The HE_{111} and EH_{111} no longer existed at the same frequency. Therefore, the absorption peak degenerated into two different parts, leading to the resonance vanishing at the same frequency.

The simulations were carried out using the commercial Lumerical FDTD Solutions. The refractive index of the silicon was $3.41 + 0.12i$. Since a thin layer high transparent PDMS was utilized, we only consider the real part of its refractive index, i.e., 1.60. The LC orientation FDTD module was applied to simulate the optical properties of the absorber along with the variation of LC directors. For the x -incident polarization, the refractive index of NJU-LDn-4 could be tuned from n_o to n_e using an electric field. Compared to the visible and near-IR range, the feature size of metamaterials in the THz region is much larger and its influence on LC anchoring can be neglected, permitting a better tunability [25]. Schematics of LC orientations in a bias saturated state is illustrated in Figure 2a. In this case, the environmental refractive index was not along x -axis. As shown in Figure 2b, a strong absorption peak (calculated from corresponding transmittance and reflectance) was observed at 0.79 THz. The side view magnetic and electric field distributions of a single unit at 0.79 THz are illustrated in Figure 2c,d. The images reveal that the magnetic dipoles lay along the y -axis while the electric dipoles lay along the x -axis. The intensity distribution indicated that both dipoles were highly localized in the silicon pillar, further facilitating the overlap of HE_{111} and EH_{111} . The impedance match was fulfilled as both the electric and magnetic resonances occurred at the same frequency [26].

After the bias was removed, the LC returned to the original orientation, as shown in Figure 3a. For the same x -incident polarization, the refractive index changed to n_e . As presented in Figure 3b, the absorption peaks of EH_{111} and HE_{111} modes separated. Their magnetic and electric field distributions at corresponding resonant frequencies are presented. The resonant frequency of the magnetic dipole was 0.81 THz, and the corresponding side view distribution is shown in Figure 3c. The resonant frequency of the electric dipole was 0.76 THz, and the distribution of the electric field in the x - z plane is shown in Figure 3d. The opposite frequency shift caused the degeneration of the absorption peak, further inducing an obvious absorption reduction. It needs to be noticed that the reduction was caused by light confinement but not the loss induced by the imaginary part variation of LC, which contributed less than 5% of total absorption change.

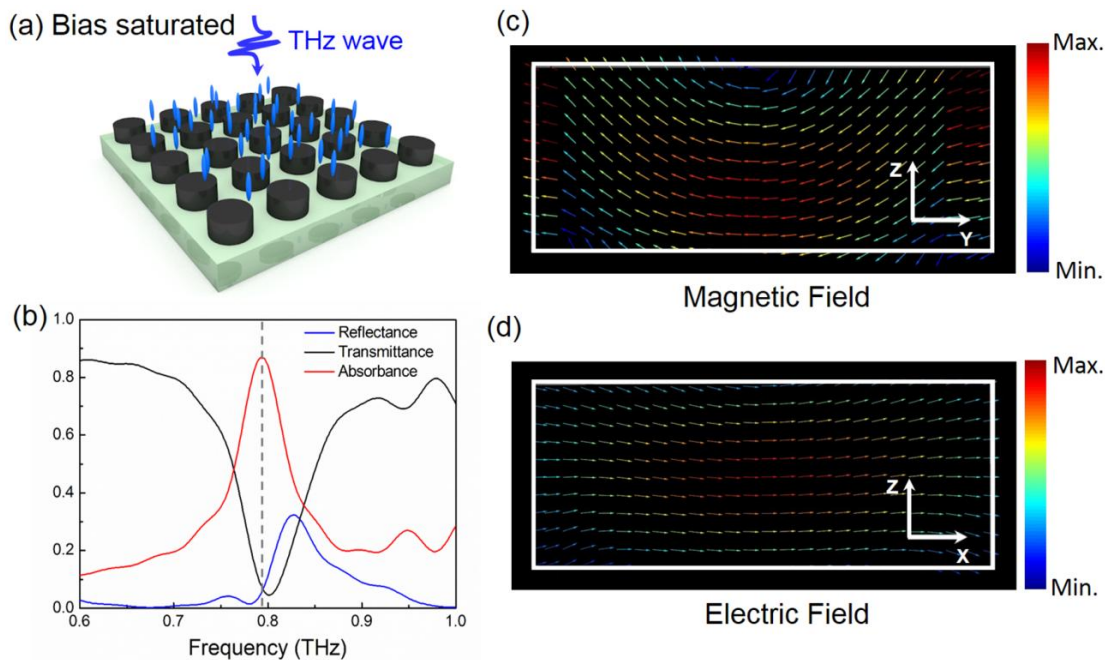


Figure 2. (a) The LC orientation in the bias saturated state. (b) Simulated spectra of reflectance, transmittance, and absorbance at bias saturated state. The (c) magnetic field of a single unit in the y - z plane, and (d) electric field in the x - z plane at 0.79 THz. The white rectangles in (c,d) represent the edge of the pillar unit, same hereinafter.

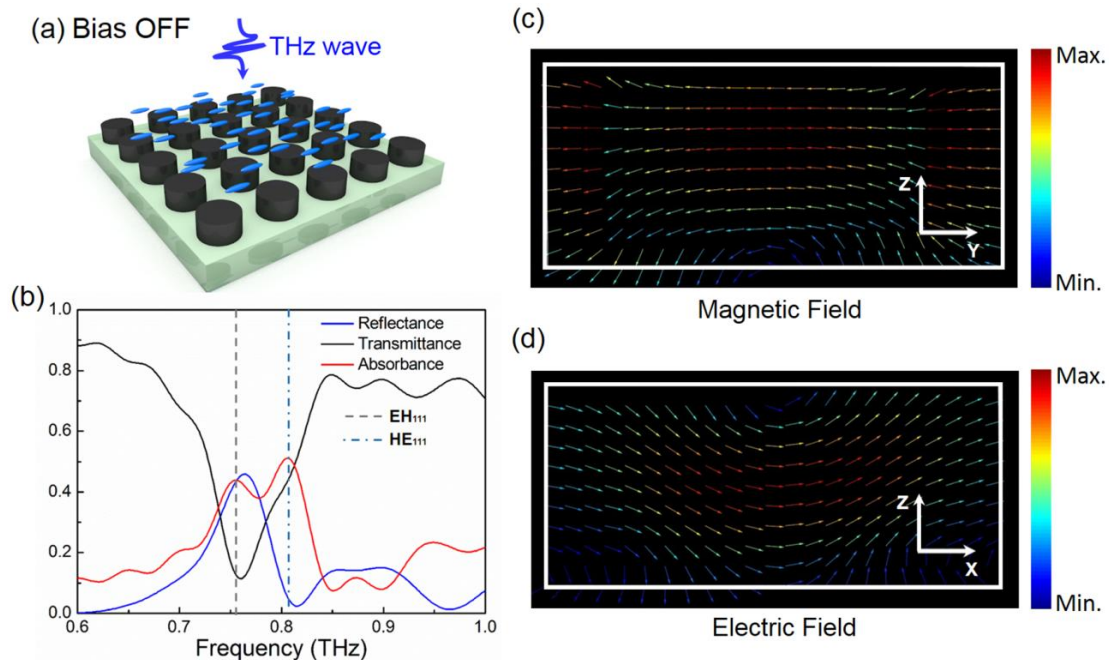


Figure 3. (a) The LC orientation in the bias OFF state. (b) Simulated spectra of reflectance, transmittance, and absorbance at bias OFF state. The (c) magnetic field of a single unit in the y - z plane at 0.81 THz, and the (d) electric field in the x - z plane at 0.76 THz.

To vividly present the evolution of the absorption peak, we depict the dependency of the EH₁₁₁ and HE₁₁₁ modes on the LC orientation (φ) in Figure 4a. The LC was set as a uniaxial medium in simulation and φ was defined as the angle between the optical axis and z-axis in the x - z plane. When $\varphi = 30^\circ$, the effective refractive index (n_{eff}) was 1.66 [27], and the absorption peak began to degenerate. As φ increased to 40° ($n_{\text{eff}} = 1.70$), the degenerated absorption peaks already existed. In this

range, the resonance was very sensitive to the refractive index change. We plot the absorbance change along φ at 0.79 THz in Figure 4b. When the refractive index changed from n_0 to n_e , a 47% decrease of absorption was achieved. The absorption was stable in the range of 0–30°. Over 30°, it changed rapidly. This means that this absorber is suitable for measuring the refractive index in this range. After 60°, the absorption changed slowly again. Additionally, since the resonance is only sensitive to the refractive index change along the incident polarization, the same LC embedded silicon pillar array is suitable for THz wave polarization detecting as well through rotating the sample. Compared to traditional broadband and frequency-tuning absorbers, our device presents the switchable absorption, which was not revealed in the former investigations. It may benefit not only the THz absorbers but also THz filters and sensors. Besides, if we set the pillar to some different radius, our design may achieve a broadband absorption in a switched OFF state and some near-unity absorption at different frequencies in a switched ON state.

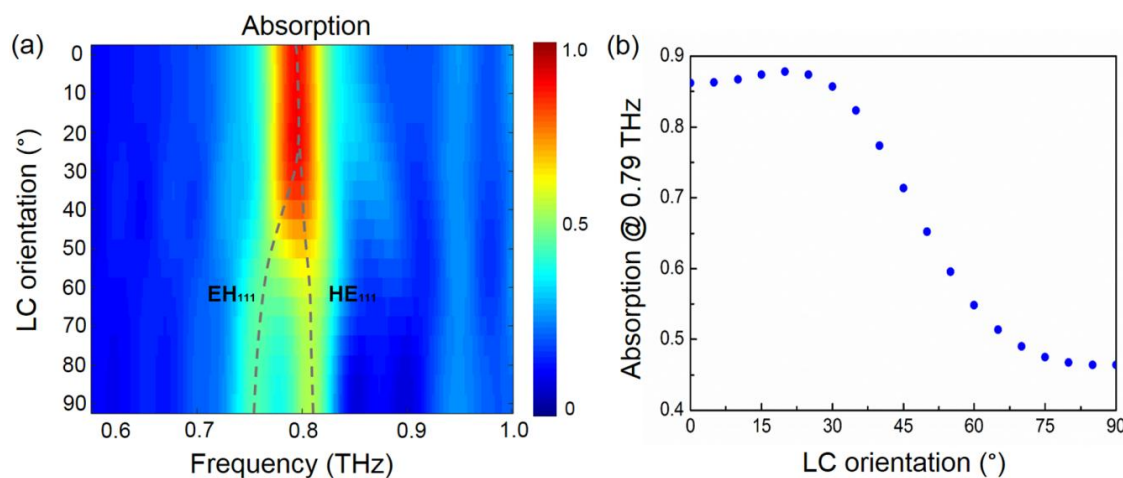


Figure 4. (a) Simulated absorption spectra along with the LC orientation changes from 0° to 90°. (b) The absorption at 0.79 THz when the LC orientation changed from 0° to 90°.

3. Conclusions

In summary, we introduced an active THz absorber composed of a silicon pillar array integrated with LC. Through spatially reorienting the LC directors with bias, its absorption peak degenerated into two small peaks, and the absorption at the resonance frequency half reduced. The proposed design adds a new candidate beyond traditional broadband and frequency tuning absorbers. The switchable absorption will benefit various applications such as energy harvesting and spatial light modulations. Also, the polarization sensitivity of the proposed device may have potential in polarization detectors. This work may supply a practical approach for active THz metadevice fabrication and may further inspire various advanced THz apparatuses in sensing, switching, imaging, and filtering.

Author Contributions: S.Z. conceived the idea of tunable metamaterial absorber and performed the numerical simulations; Z.S. and R.K. analyzed the simulations and modified the article; S.G. and W.H. supervised the whole work.

Funding: This research was supported by the National Key Research and Development Program of China (2017YFA0303700), the National Natural Science Foundation of China (NSFC) (Nos. 61575093, 61490714, and 61435008), the Distinguished Young Scholars Fund of Jiangsu Province (BK20180004), the Fundamental Research Funds for the Central Universities, and Jiangsu Donghai Silicon Industry Science and Technology Innovation Center.

Conflicts of Interest: The authors declare no conflict of interest.

References

- Grossman, E.; Dietlein, C.; Ala-Laurinaho, J.; Leivo, M.; Gronberg, L.; Gronholm, M.; Lappalainen, P.; Rautiainen, A.; Tamminen, A.; Luukanen, A. Passive terahertz camera for standoff security screening. *Appl. Opt.* **2010**, *49*, E106–E120. [[CrossRef](#)] [[PubMed](#)]
- John, F.F.; Brian, S.; Feng, H.; Dale, G.; Robert, B.; Filipe, O.; David, Z. THz imaging and sensing for security applications—Explosives, weapons and drugs. *Semicond. Sci. Technol.* **2005**, *20*, S266. [[CrossRef](#)]
- Ferguson, B.; Zhang, X.-C. Materials for terahertz science and technology. *Nat. Mater.* **2002**, *1*, 26. [[CrossRef](#)] [[PubMed](#)]
- Fei, D.; Anders, P.; Sergey, I.B. Gradient metasurfaces: A review of fundamentals and applications. *Rep. Prog. Phys.* **2018**, *81*, 026401. [[CrossRef](#)]
- Tao, H.; Landy, N.I.; Bingham, C.M.; Zhang, X.; Averitt, R.D.; Padilla, W.J. A metamaterial absorber for the terahertz regime: Design, fabrication and characterization. *Opt. Express* **2008**, *16*, 7181–7188. [[CrossRef](#)] [[PubMed](#)]
- Shrekenhamer, D.; Chen, W.-C.; Padilla, W.J. Liquid Crystal Tunable Metamaterial Absorber. *Phys. Rev. Lett.* **2013**, *110*, 177403. [[CrossRef](#)] [[PubMed](#)]
- Driscoll, T.; Kim, H.-T.; Chae, B.-G.; Kim, B.-J.; Lee, Y.-W.; Jokerst, N.M.; Palit, S.; Smith, D.R.; Di Ventra, M.; Basov, D.N. Memory Metamaterials. *Science* **2009**, *325*, 1518–1521. [[CrossRef](#)] [[PubMed](#)]
- Chen, H.-T.; Padilla, W.J.; Zide, J.M.O.; Gossard, A.C.; Taylor, A.J.; Averitt, R.D. Active terahertz metamaterial devices. *Nature* **2006**, *444*, 597. [[CrossRef](#)] [[PubMed](#)]
- Lee, S.H.; Choi, M.; Kim, T.-T.; Lee, S.; Liu, M.; Yin, X.; Choi, H.K.; Lee, S.S.; Choi, C.-G.; Choi, S.-Y.; et al. Switching terahertz waves with gate-controlled active graphene metamaterials. *Nat. Mater.* **2012**, *11*, 936. [[CrossRef](#)] [[PubMed](#)]
- Savo, S.; Shrekenhamer, D.; Padilla, W.J. Liquid Crystal Metamaterial Absorber Spatial Light Modulator for THz Applications. *Adv. Opt. Mater.* **2014**, *2*, 275–279. [[CrossRef](#)]
- Shen, Z.; Zhou, S.; Ge, S.; Duan, W.; Chen, P.; Wang, L.; Hu, W.; Lu, Y. Liquid-crystal-integrated metadevice: Towards active multifunctional terahertz wave manipulations. *Opt. Lett.* **2018**, *43*, 4695–4698. [[CrossRef](#)] [[PubMed](#)]
- Liu, X.; Fan, K.; Shadrivov, I.V.; Padilla, W.J. Experimental realization of a terahertz all-dielectric metasurface absorber. *Opt. Express* **2017**, *25*, 191–201. [[CrossRef](#)] [[PubMed](#)]
- Wang, L.; Lin, X.-W.; Hu, W.; Shao, G.-H.; Chen, P.; Liang, L.-J.; Jin, B.-B.; Wu, P.-H.; Qian, H.; Lu, Y.-N.; et al. Broadband tunable liquid crystal terahertz waveplates driven with porous graphene electrodes. *Light Sci. Appl.* **2015**, *4*, e253. [[CrossRef](#)]
- Ge, S.; Chen, P.; Shen, Z.; Sun, W.; Wang, X.; Hu, W.; Zhang, Y.; Lu, Y. Terahertz vortex beam generator based on a photopatterned large birefringence liquid crystal. *Opt. Express* **2017**, *25*, 12349–12356. [[CrossRef](#)] [[PubMed](#)]
- Kowerdziej, R.; Olifierczuk, M.; Parka, J.; Wrobel, J. Terahertz characterization of tunable metamaterial based on electrically controlled nematic liquid crystal. *Appl. Phys. Lett.* **2014**, *105*, 022908. [[CrossRef](#)]
- Chen, C.C.; Chiang, W.F.; Tsai, M.C.; Jiang, S.A.; Chang, T.H.; Wang, S.H.; Huang, C.Y. Continuously tunable and fast-response terahertz metamaterials using in-plane-switching dual-frequency liquid crystal cells. *Opt. Lett.* **2015**, *40*, 2021–2024. [[CrossRef](#)] [[PubMed](#)]
- Borislav, V.; Dimitrios, C.Z.; Goran, I.; Romeo, B.; Radoš, G. Electrically tunable terahertz polarization converter based on overcoupled metal-isolator-metal metamaterials infiltrated with liquid crystals. *Nanotechnology* **2017**, *28*, 124002. [[CrossRef](#)]
- Ji, Y.-Y.; Fan, F.; Chen, M.; Yang, L.; Chang, S.-J. Terahertz artificial birefringence and tunable phase shifter based on dielectric metasurface with compound lattice. *Opt. Express* **2017**, *25*, 11405–11413. [[CrossRef](#)] [[PubMed](#)]
- Tang, K.C.; Liao, E.; Ong, W.L.; Wong, J.D.S.; Agarwal, A.; Nagarajan, R.; Yobas, L. Evaluation of bonding between oxygen plasma treated polydimethyl siloxane and passivated silicon. *J. Phys. Conf. Ser.* **2006**, *34*, 155. [[CrossRef](#)]
- Chen, P.; Ma, L.-L.; Duan, W.; Chen, J.; Ge, S.-J.; Zhu, Z.-H.; Tang, M.-J.; Xu, R.; Gao, W.; Li, T.; et al. Digitalizing Self-Assembled Chiral Superstructures for Optical Vortex Processing. *Adv. Mater.* **2018**, *30*, 1705865. [[CrossRef](#)] [[PubMed](#)]

21. Wang, L.; Lin, X.-W.; Liang, X.; Wu, J.-B.; Hu, W.; Zheng, Z.-G.; Jin, B.-B.; Qin, Y.-Q.; Lu, Y.-Q. Large birefringence liquid crystal material in terahertz range. *Opt. Mater. Express* **2012**, *2*, 1314–1319. [[CrossRef](#)]
22. Mongia, R.K.; Bhartia, P. Dielectric resonator antennas—A review and general design relations for resonant frequency and bandwidth. *Int. J. Microw. Millim.-Wave Comput.-Aided Eng.* **1994**, *4*, 230–247. [[CrossRef](#)]
23. Decker, M.; Staude, I.; Falkner, M.; Dominguez, J.; Neshev, D.N.; Brener, I.; Pertsch, T.; Kivshar, Y.S. High-Efficiency Dielectric Huygens’ Surfaces. *Adv. Opt. Mater.* **2015**, *3*, 813–820. [[CrossRef](#)]
24. Fan, K.; Suen, J.Y.; Liu, X.; Padilla, W.J. All-dielectric metasurface absorbers for uncooled terahertz imaging. *Optica* **2017**, *4*, 601–604. [[CrossRef](#)]
25. Buchnev, O.; Podoliak, N.; Kaczmarek, M.; Zheludev, N.I.; Fedotov, V.A. Metamaterials: Electrically Controlled Nanostructured Metasurface Loaded with Liquid Crystal: Toward Multifunctional Photonic Switch (Advanced Optical Materials 5/2015). *Adv. Opt. Mater.* **2015**, *3*, 595. [[CrossRef](#)]
26. Staude, I.; Miroshnichenko, A.E.; Decker, M.; Fofang, N.T.; Liu, S.; Gonzales, E.; Dominguez, J.; Luk, T.S.; Neshev, D.N.; Brener, I.; et al. Tailoring Directional Scattering through Magnetic and Electric Resonances in Subwavelength Silicon Nanodisks. *ACS Nano* **2013**, *7*, 7824–7832. [[CrossRef](#)] [[PubMed](#)]
27. Yeh, P. Optics of Liquid Crystal Displays. In Proceedings of the Conference on Lasers and Electro-Optics—Pacific Rim (CLEO/Pacific Rim 2007), Seoul, Korea, 26 August 2007.



© 2018 by the authors. Licensee MDPI, Basel, Switzerland. This article is an open access article distributed under the terms and conditions of the Creative Commons Attribution (CC BY) license (<http://creativecommons.org/licenses/by/4.0/>).